JCB Article

# A fluorescent resonant energy transfer–based biosensor reveals transient and regional myosin light chain kinase activation in lamella and cleavage furrows

**Teng-Leong Chew,[1] Wendy A. Wolf,[1] Patricia J. Gallagher,[2] Fumio Matsumura,[3] and Rex L. Chisholm[1]**

[1]Department of Cell and Molecular Biology, R.H. Lurie Comprehensive Cancer Center and Center for Genetic Medicine, Northwestern University Medical School, Chicago, IL 60611
[2]Department of Physiology, Indiana University School of Medicine, Indianapolis, IN 46202
[3]Department of Molecular Biology and Biochemistry, Rutgers University, Nelson Labs, Busch Campus, Piscataway, NJ 08855



Approaches with high spatial and temporal resolution are required to understand the regulation of nonmuscle myosin II in vivo. Using fluorescence resonance energy transfer we have produced a novel biosensor allowing simultaneous determination of myosin light chain kinase (MLCK) localization and its $[Ca^{2+}]_4$/calmodulin-binding state in living cells. We observe transient recruitment of diffuse MLCK to stress fibers and its in situ activation before contraction. MLCK is highly active in the lamella of migrating cells, but not at the retracting tail. This unexpected result highlights a potential role for MLCK-mediated myosin contractility in the lamella as a driving force for migration. During cytokinesis, MLCK was enriched at the spindle equator during late metaphase, and was maximally activated just before cleavage furrow constriction. As furrow contraction was completed, active MLCK was redistributed to the poles of the daughter cells. These results show MLCK is a myosin regulator in the lamella and contractile ring, and pinpoints sites where myosin function may be mediated by other kinases.

## Introduction

Phosphorylation of the 20-kD regulatory light chain (RLC)* regulates nonmuscle myosin II activity. RLC phosphorylation sites can be categorized into inhibitory and activating based on their effects on myosin function. Phosphorylation of Ser-19 and Thr-18 stimulates myosin activity, whereas Ser-1, Ser-2, and Thr-9 phosphorylation is inhibitory. Ser-19 can be phosphorylated by several kinases, including myosin light chain kinase (MLCK) (Sellers et al., 1981; Ikebe et al., 1986), Rho kinase (Amano et al., 1996), and p21-activated kinase (PAK) (Chew et al., 1998; Zeng et al., 2000). MLCK also phosphorylates RLC at Thr-18 (Ikebe et al., 1986). Thr18-ser19 diphosphorylation maximally activates myosin ATPase in vitro (Sellers et al., 1981), and produces maximal isometric tension development in thrombin-stimulated endothelial cells (Goeckeler and Wysolmerski, 1995). Phosphorylation of RLC at Ser-1, Ser-2, or Thr-9 by protein kinase C (Ikebe et al., 1987) or Cdc2 kinase (Satterwhite et al., 1992; Mishima and Mabuchi, 1996) inhibits myosin activity and decreases the Km of MLCK for RLC (Turbedsky et al., 1997).

The kinases that phosphorylate the RLC are regulated by distinct upstream signals, such as $[Ca^{2+}]_4$/calmodulin and Rho family GTPases. In addition, many of these pathways interact. For example, cdc42-activated PAK phosphorylates RLC at Ser-19 (Chew et al., 1998; Zeng et al., 2000) and inhibits MLCK, preventing Thr-18 phosphorylation (Sanders et al., 1999; Goeckeler et al., 2000). This complexity suggests that cells spatially and temporally compartmentalize their signals. How these different kinases are targeted to their sites of action remains unre-

The online version of this paper contains supplemental material.

Address correspondence to Rex L. Chisholm, Department of Cell and Molecular Biology, 303 E. Chicago Ave., Northwestern University Medical School, Chicago, IL 60611. Tel.: (312) 503-4151. Fax: (312) 503-5994. E-mail: r-chisholm@nwu.edu

*Abbreviations used in this paper: BFP, blue fluorescent protein; CBD, calmodulin binding domain; FIP, fluorescent indicator protein; FRET, fluorescent resonant energy transfer; GFP, green fluorescent protein; MLCK, myosin light chain kinase; PAK, p21-activated kinase; RLC, regulatory light chain.

Key words: myosin light chain kinase; myosin light chains; phosphorylation; cell division; FRET

solved, in part due to our inability to follow these molecular events dynamically.

MLCK is a $[Ca^{2+}]_4$/calmodulin-dependent kinase implicated in nonmuscle contraction (Goeckeler and Wysolmerski, 1995), cytokinesis (Poperechnaya et al., 2000), stress fiber formation (Chrzanowska-Wodnicka and Burridge, 1996), and motility (Kishi et al., 2000). The MLCK gene encodes two different kinases, a 210-kD MLCK ($MLCK_{210}$) expressed primarily in nonmuscle cells, and a differentially spliced isoform of 108–125 kD, $MLCK_{125}$ (Poperechnaya et al., 2000). Although previous immunolocalization studies have localized MLCK to stress fibers as well as the cleavage furrow of dividing cells (de Lanerolle et al., 1981; Guerriero et al., 1981), the dynamics of MLCK activation in these regions is unknown. The formation and maintenance of stress fibers are believed to require RLC phosphorylation (Chrzanowska-Wodnicka and Burridge, 1996), consistent with the stress fiber association of MLCK. However, despite localization of MLCK to stress fibers, myosin is not fully activated as further contraction can be induced. This suggests myosin can be further potentiated to produce maximal contraction. In addition, we do not know if MLCK activation precedes or follows stress fiber localization. The convergence of multiple signals on myosin highlights the possibility of regionalized myosin regulation by distinct pathways. These unresolved issues underscore the need to dissect these pathways spatially and temporally. As the best characterized RLC kinase, MLCK is an ideal target for dynamic localization of activation state.

Using fluorescence resonant energy transfer (FRET) between blue (BFP) and green (GFP) fluorescent proteins, Romoser et al. (1997) developed a fluorescent indicator protein (FIP) that detected $[Ca^{2+}]_4$/calmodulin changes in live cells. Here we report the engineering of a novel biosensor, created by fusing the FIP to the MLCK COOH terminus, that detects the calmodulin binding state of MLCK. Since $[Ca^{2+}]_4$/calmodulin-binding activates MLCK, this sensor provides a representation of the activation state of MLCK. Using this approach, we observed that localized MLCK activation along stress fibers precedes cell contraction, demonstrating that MLCK activity can be modulated in situ on stress fibers to mediate the extent of myosin contractility. Activated

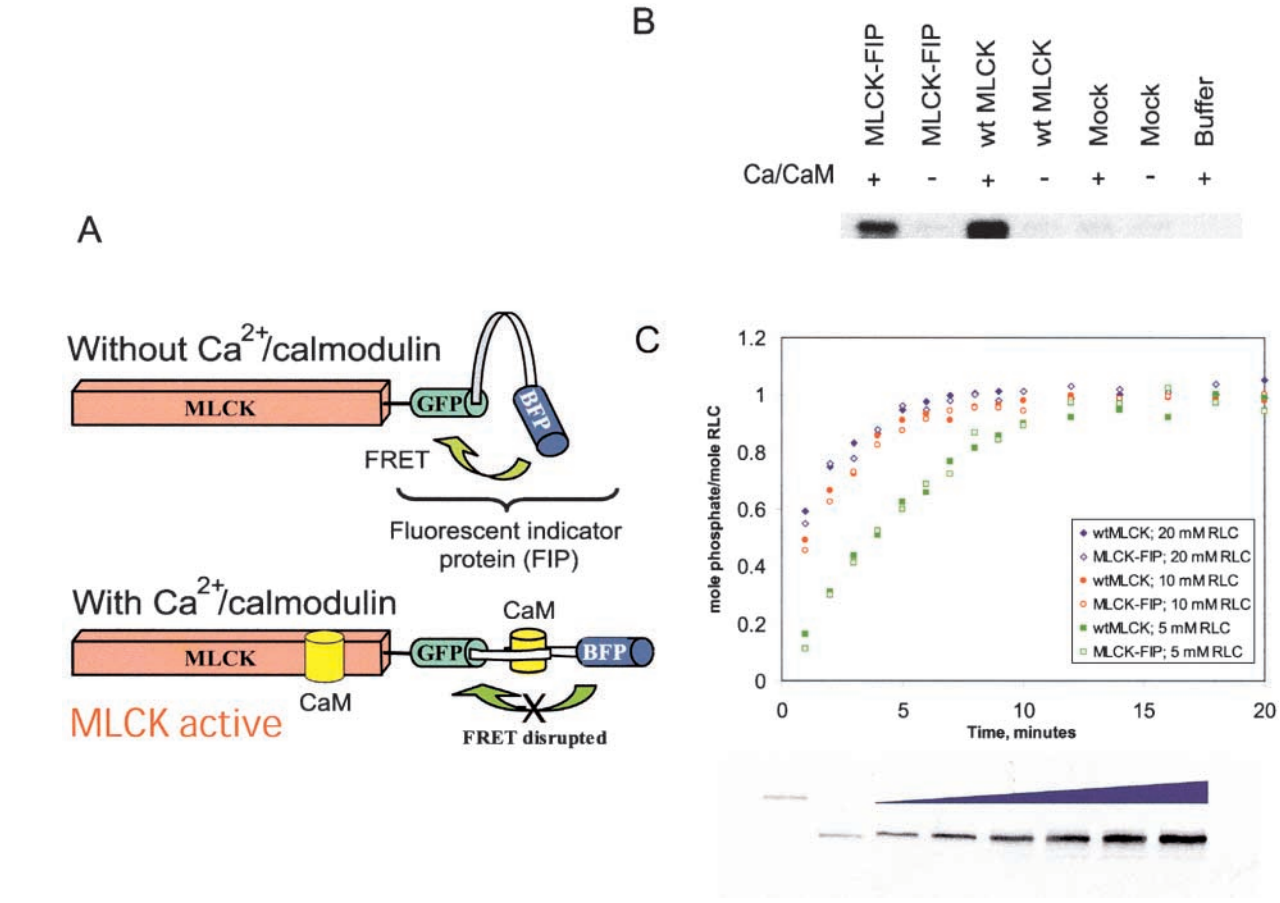


Figure 1. **MLCK-FIP is a FRET-based $[Ca^{2+}]_4$/calmodulin sensor with activity and regulation similar to wild-type MLCK.** (A) Schematic diagram of MLCK-FIP. The fluorescent indicator protein (FIP) consists of BFP linked to GFP via the $[Ca^{2+}]_4$/calmodulin-binding domain derived from MLCK. In the absence of $[Ca^{2+}]_4$/calmodulin, the coiled $[Ca^{2+}]_4$/calmodulin binding domain allows FRET between the fluorophores. When $[Ca^{2+}]_4$/calmodulin (yellow cylinder) is present, it binds and activates MLCK and binds between the fluorophores disrupting FRET. (B) MLCK-FIP shows $[Ca^{2+}]_4$/calmodulin dependent kinase activity. Lysates from mock-transfected COS-7 cells or cells transiently expressing MLCK-FIP, wild-type MLCK were tested for their ability to phosphorylate RLC in a $[Ca^{2+}]_4$/calmodulin-dependent fashion. Endogenous kinase activity was evident only after prolonged exposure of the autoradiograph. (C) MLCK-FIP phosphorylates RLC at rates similar to wild-type MLCK. The activity of immunoprecipitated MLCK-FIP and wild-type MLCK was tested using three RLC concentrations. Amounts of immunoprecipitated kinase were determined using a standard curve of known MLCK concentrations detected by anti-MLCK pAb (bottom).

MLCK was also observed within the protruding lamella, localizing activated MLCK to where significant myosin reorganization occurs. During cell division, MLCK was enriched at the spindle equator during metaphase and at the poles of the daughter cells as cleavage furrow contraction was completed. In addition, observation of areas where MLCK is under represented identifies sites where myosin activity may be regulated by other pathways.

## Results

### Construction of a sensor to detect MLCK localization and calmodulin binding state

MLCK is activated by calmodulin binding. To detect calmodulin binding to MLCK, the FIP was linked to the MLCK COOH terminus. In the absence of bound calmodulin, the coiled conformation of the calmodulin binding domain (CBD) linking the BFP and GFP facilitates FRET upon BFP excitation (Fig. 1 A). When MLCK-FIP encounters increased concentrations of $[Ca^{2+}]_4$/calmodulin, the CBD in both MLCK and the FIP bind calmodulin, changing its conformation, activating MLCK, and disrupting FRET. By exciting BFP and monitoring the emission from GFP, the subcellular localization and the calmodulin-binding state of MLCK can be simultaneously monitored in living cells, allowing us to infer MLCK activation state.

### MLCK-FIP has wild-type calmodulin-dependent RLC kinase activity

To test the regulation of MLCK-FIP, we assessed its ability to phosphorylate RLC. Lysates from COS-7 cells overexpressing either wild-type MLCK or MLCK-FIP were incubated with RLC. In the presence of $[Ca^{2+}]_4$/calmodulin, lysates from wild-type MLCK and MLCK-FIP showed significantly higher activities than mock-transfected cell lysates or when $Ca^{2+}$ was omitted (Fig. 1 B). This result demonstrated the $[Ca^{2+}]_4$/calmodulin dependence of the MLCK-FIP, showing that the FIP did not interfere with normal MLCK regulation.

To assess the enzymatic properties of MLCK-FIP, we compared the rates of RLC phosphorylation mediated by MLCK-FIP or wild-type MLCK at three different subsaturating RLC concentrations. This approach was necessary because the bacterially expressed RLC precipitated at high concentration, limiting our ability to determine MLCK kinetics at high RLC concentrations. MLCK-FIP and wild-type MLCK were expressed in COS-7 cells and immunoprecipitated using an MLCK-specific antibody. The amount of recombinant MLCK-FIP and wild-type MLCK was determined by comparing their intensity on an immunoblot to that of a standard curve (Fig. 1 C, bottom). Since endogenous kinase activity was not detected, the activity in the immunoprecipitates represented the expressed kinase activity (a faint endogenous band of $MLCK_{125}$ was evident only after prolonged exposure, unpublished data). Immunoprecipitates containing equal amounts of wild-type MLCK and MLCK-FIP were used in the in vitro kinase assay. Fig. 1 C shows that both wild-type MLCK and MLCK-FIP phosphorylate RLC at indistinguishable rates at all three substrate concentrations tested. Since the recombinant RLC was buffered in high salt to prevent precipitation, both wild-type MLCK and MLCK-FIP–phosphorylated RLC to a maximum of 1 mol phosphate incorporated per mole RLC, consistent with previous findings that the MLCK-mediated diphosphorylation of RLC is sensitive to high ionic strength (Ikebe and Hartshorne, 1985). These results demonstrate

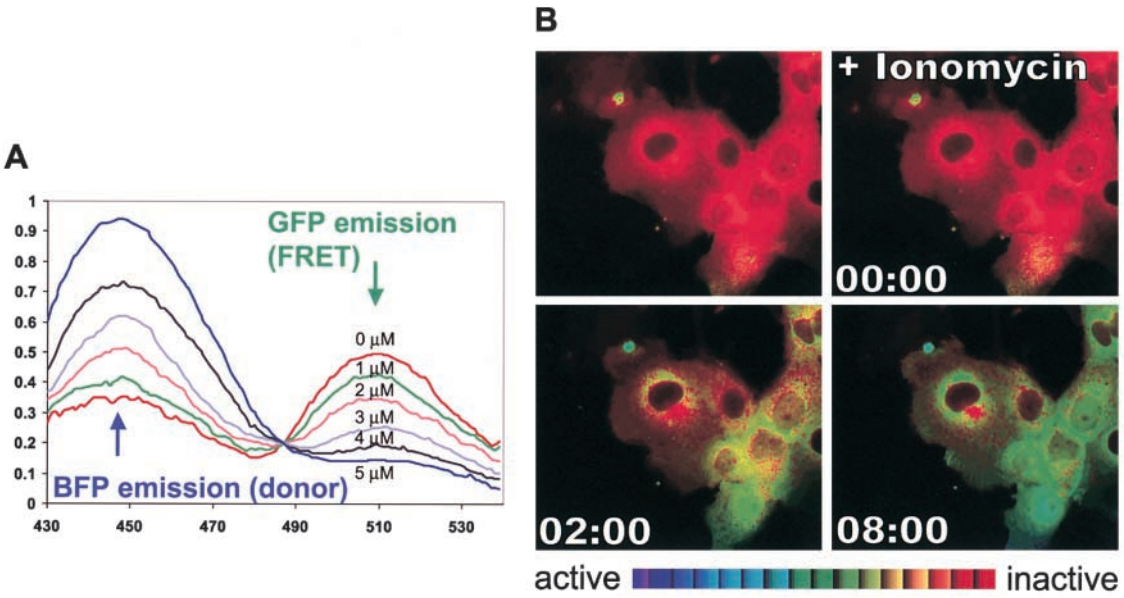


Figure 2. **MLCK-FIP detects $[Ca^{2+}]_4$/calmodulin changes in vitro and in vivo.** (A) Partially purified MLCK-FIP in buffer containing 1 μM calmodulin was exposed to increasing free $Ca^{2+}$. Emission scans (using 380 nm excitation) were obtained at increasing $CaCl_2$ concentrations. (B) COS-7 cells overexpressing MLCK-FIP were treated with 1 μM ionomycin, and ratio imaging used to monitor the $[Ca^{2+}]_4$/calmodulin binding to MLCK-FIP. Relative $[Ca^{2+}]_4$/calmodulin binding (representing MLCK activity) is displayed using intensity-modulated display with blue indicating bound calmodulin (active MLCK) and red showing little bound calmodulin (inactive MLCK) as shown in the ratio bar.

that MLCK-FIP has the same $[Ca^{2+}]_4$/calmodulin-dependent kinase activity as wild-type MLCK.

### MLCK-FIP detects changes in $[Ca^{2+}]_4$/calmodulin concentrations in vitro

Next, we ascertained the ability of MLCK-FIP to detect $[Ca^{2+}]_4$/calmodulin changes in vitro. MLCK-FIP was purified, and the emission spectrum was determined following excitation at 380 nm in the presence of increasing amounts of $CaCl_2$. Fig. 2 A shows that MLCK-FIP displays decreased FRET, detected by decreased 509 nm emission, in response to increased $[Ca^{2+}]$ concentration. Decreased GFP emission was accompanied by a corresponding increase in BFP emission (448 nm), consistent with loss of FRET. This result, consistent with the behavior of FIP (Romoser et al., 1997), shows that MLCK-FIP effectively detects changes in $[Ca^{2+}]_4$/calmodulin concentration.

### MLCK-FIP detects $[Ca^{2+}]_4$/calmodulin changes in vivo

The simultaneous monitoring of MLCK localization and $[Ca^{2+}]_4$/calmodulin binding requires two measurements, one to determine the amount of FRET (corresponding to activity state) and a second to determine MLCK-FIP intensity (corresponding to distribution). Relative MLCK activity ($[Ca^{2+}]_4$/calmodulin binding state) is represented by a ratio of intensity from the FRET acceptor (GFP emission at 510 nm caused by stimulation of the donor at 380 nm), $F_{FRET}$, divided by the intensity of the acceptor (at 510 nm) produced by direct stimulation of the acceptor (at 460 nm), $F_{GFP}$. Since $F_{GFP}$ is obtained by direct excitation of the GFP, the intensity is not affected by FRET, thus providing an independent measurement of MLCK concentration. However, it is important to note that $F_{GFP}$ cannot distinguish between changes in path length and MLCK concentration. Regions with significant difference in thickness will have difference in $F_{GFP}$ intensities. Caution needs to be applied when comparing MLCK concentration in cellular regions with significant difference in thickness.

To test MLCK-FIP detection of $[Ca^{2+}]_4$/calmodulin changes in live cells, MLCK-FIP spectra were monitored following $Ca^{2+}$ ionophore, ionomycin, treatment of MLCK-FIP transfected COS-7 cells. COS-7 cells were chosen because they significantly overexpress recombinant proteins and have high transfection efficiency. As shown in Fig. 2 B, the high protein expression level resulted in a generally diffuse localization of MLCK-FIP. Prior to the ionomycin treatment, ratio images indicate that MLCK-FIP was not in the calmodulin-bound state (red, MLCK inactive). A dramatic loss of FRET was seen immediately after ionomycin treatment (Fig. 2 B), indicated by a shift from red to green or blue, showing that MLCK-FIP bound calmodulin and was therefore activated. This result shows that MLCK-FIP detects $[Ca^{2+}]_4$/calmodulin changes in live cells. It also shows that there was sufficient calmodulin to allow MLCK-FIP to detect increased $[Ca^{2+}]_4$/calmodulin binding even when MLCK-FIP was overexpressed.

The data in Fig. 2 B is displayed using Intensity-Modulated Display (IMD) (Tsien and Harootunian, 1990), in which the FRET/GFP ratio determines color, and the intensity of the $F_{GFP}$ determines the color intensity. In this method, the pixel values 0–255 are divided into 16 bins (0–15, 16–31, etc.) to represent FRET levels. Within each bin, the lowest number represents the lowest $F_{GFP}$ intensity while the highest number represents the highest intensity. For example, in the 0–15 bin representing the smallest FRET ratio, a pixel value of 0 would represent a small amount of calmodulin-bound MLCK (activated), while 15 would represent a large amount of calmodulin bound MLCK. Similarly, in the 240–255 bin (representing the highest FRET and therefore the lowest amount of bound calmodulin or relatively inactive kinase) a value of 240 represents little inactive kinase while 255 represents a large amount of inactive kinase. This mathematical manipulation provides a dynamic two-dimensional display of MLCK regulation.

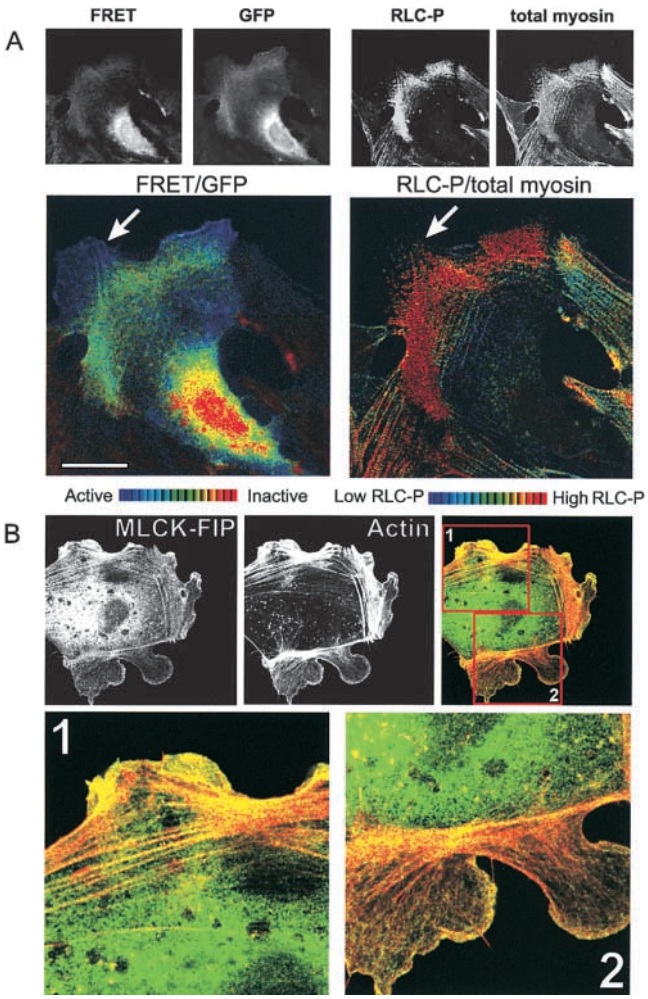


Figure 3. **MLCK-FIP associates with stress fibers and highlights areas of increased RLC phosphorylation.** (A) The distribution of RLC phosphorylation was assessed by determining the ratio of phosphorylated RLC to total myosin (right) and displayed according to the ratio bar (bottom right). Myosin with highly phosphorylated RLC is indicated in red. MLCK-FIP localization and activity are shown in the left panel. Arrows highlight regions of lamellipodia where high kinase activity colocalizes with myosin spots. (B) Colocalization of MLCK-FIP and rhodamine phallodin–stained stress fibers. Bar, 5 μm.

### Regions with MLCK-FIP activation exhibit highly phosphorylated RLC

If MLCK-FIP accurately reflects the activation state of MLCK, cellular regions with $[Ca^{2+}]_4$/calmodulin-bound

MLCK should correspond with regions of increased RLC phosphorylation. To test this, we compared the MLCK-FIP ratio image with the distribution of phosphorylated RLC using a polyclonal antibody specific for RLC phospho-Ser-19 (Matsumura et al., 1998). PTK-2 cells expressing MLCK-FIP were imaged to obtain a $F_{FRET}/F_{GFP}$ ratio (Fig. 3 A, left), then immediately fixed and double-stained for myosin heavy chain and phosphorylated RLC. The level of RLC phosphorylation is displayed as a ratio of phosphorylated RLC to total myosin (Fig. 3 A, right). Myosin associated with stress fibers throughout lamella had highly phosphorylated RLC. The $F_{FRET}/F_{GFP}$ ratio image shows a strong correlation between $MLCK_{125}$ activation and RLC phosphorylation. In addition, the MLCK-FIP suggests that MLCK is highly active within the lamella where very little myosin was observed. In this region, myosin is organized into clusters of bipolar filaments that appear as spots undergoing retrograde movement (Verkhovsky and Borisy, 1993; Verkhovsky et al., 1995). This pattern of myosin organization within lamella suggests that there is a pool of diffuse myosin that becomes more highly organized. The fact that MLCK-FIP is highly activated in this region suggests that active $MLCK_{125}$ may mediate this myosin reorganization.

Our results suggested that $MLCK_{125}$ localized to stress fibers. To confirm this, we assessed colocalization of MLCK-FIP and F-actin by comparing the MLCK-FIP image with rhodamine-phalloidin staining of fixed cells. Fig. 3 B clearly shows the colocalization of MLCK-FIP with phalloidin stained stress fibers.

## Localized MLCK activation precedes regional cellular contraction

MLCK activation has been implicated in nonmuscle cell contraction (Goeckeler and Wysolmerski, 1995) and correlates with isometric tension development in permeabilized endothelial cells (Wysolmerski and Lagunoff, 1991). We examined how MLCK–calmodulin interaction correlated with cell contraction in transiently transfected PTK-2 cells. PTK-2 cells were used because of their high transfection efficiency, prominent stress fiber network, and the fact that they express MLCK-FIP at significantly lower levels than COS-7 cells, whose ultra-high expression level would have interfered with the imaging of cytoskeletal structures. Fig. 4 shows two different examples of contracting PTK2 cells. Cell contraction was characterized by stress fibers shortening and decreased cell margins. The $F_{FRET}/F_{GFP}$ ratios are displayed in a three-dimensional plot with color indicating MLCK activity state as shown in the ratio bar (bottom), and height indicating fluorescence intensity of directly stimulated GFP. Regions with abundant MLCK-FIP are represented by peaks of

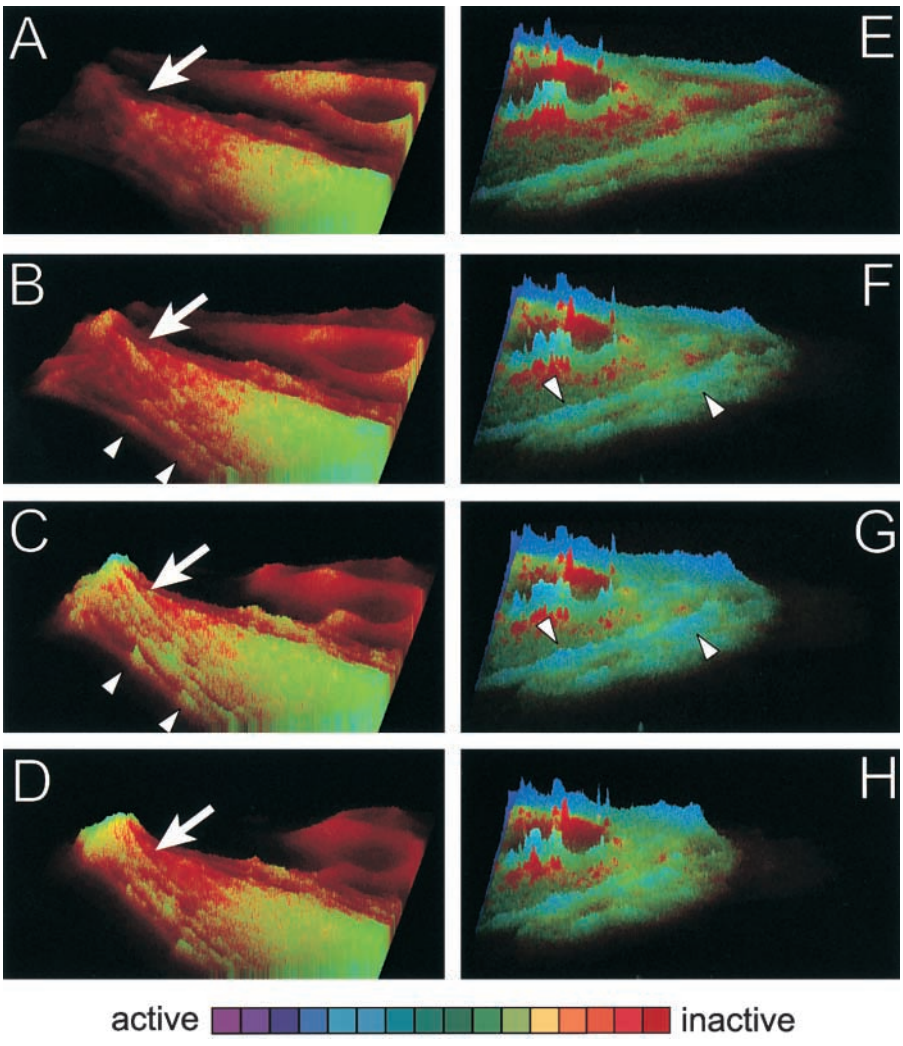


Figure 4. **Transient recruitment and activation of $MLCK_{125}$ along contracting stress fibers.** Ratio images of two contracting cells (out of four observed). The intensity of MLCK-FIP is represented by the peak height (high peaks indicate enrichment of MLCK) while the MLCK-FIP $[Ca^{2+}]_4$/calmodulin-binding state is displayed by the color. Red (high ratio) represents inactive kinase, while blue indicates $[Ca^{2+}]_4$/calmodulin-bound kinase. Arrows indicate regions where diffuse MLCK is recruited to stress fibers, and arrow heads show sites of in situ activation of MLCK-FIP. Please refer to Videos 1 and 2 (available at http://www.jcb.org/cgi/content/full/jcb.200110161/DC1) for the dynamic MLCK profile.

increased height. Fig. 4, A–D, (and Video 1) shows that transient and highly localized $MLCK_{125}$ enrichment and apparent activation along stress fibers precedes cellular contraction. Diffuse MLCK–FIP (Fig. 4 A) became increasingly associated with stress fibers before contraction (Fig. 4, B and C, arrows). MLCK–FIP also showed regulated activity in situ along stress fibers (Fig. 4, B–D, arrowheads), where the activity first increased at the start of contraction, then decreased as contraction ends. Fig. 4, E–H (Video 2), show another example. These results demonstrate that $MLCK_{125}$ can associate with stress fibers, although based on previous results (Poperechnaya et al., 2000) its association with the cytoskeleton may be more transient than that of $MLCK_{210}$. Videos are available at http://www.jcb.org/cgi/content/full/jcb.200110161/DC1.

### $MLCK_{125}$ is activated in the lamella of migrating cells

Since $MLCK_{125}$ bound calmodulin in the lamella of stationary cells, we investigated its behavior in the extending lamella of PTK2 cells stimulated to migrate by hepatocyte growth factor/scatter factor. Fig. 5 suggests MLCK activation in the lamella of motile PTK-2 cells based on increased calmodulin binding. Since the $F_{FRET}$ image and the $F_{GFP}$ image are taken sequentially, we worried that movement might create a motion artifact that could be misinterpreted as a loss of FRET (MLCK activation). Two lines of evidence argue against this. First, extending lamellas continue to show active MLCK-FIP (Fig. 3) after fixation. Second, alternating the order of collection of the FRET and GFP images did not alter the MLCK-FIP activation profile (unpublished data).

MLCK-FIP in the lamella associated with a meshwork resembling actin, consistent with $MLCK_{125}$ binding to F-actin. The level of MLCK activation was consistently higher in the leading lamella than the retracting tail (eight out of nine cells observed), where myosin contractility has been postulated to dislodge focal adhesions during cell movement. Previous studies (Matsumura et al., 1998) showed elevated RLC phosphorylation in the tail, raising the possibility that MLCK may not be responsible for phosphorylating RLC in the tail. Perhaps one of the other RLC-targeting kinases regulates myosin at the retracting tail.

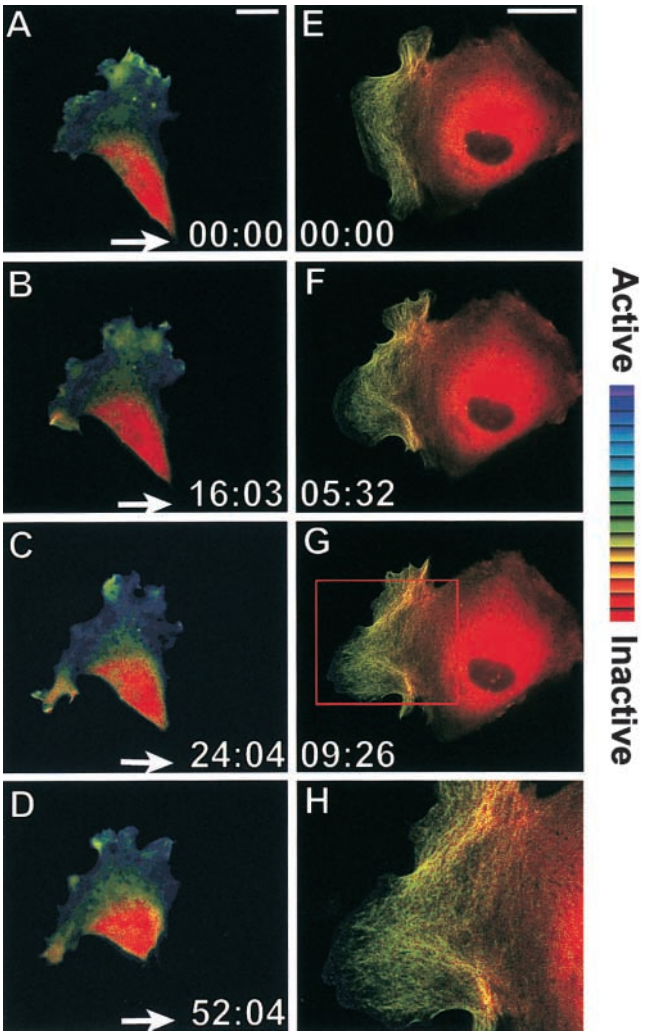


Figure 5. **$MLCK_{125}$ is activated in the lamella. MLCK-FIP shows the binding of $[Ca^{2+}]_4$/calmodulin to MLCK within the protruding lamella of motile (A–D) and stationary (E–H) PTK-2 cells.** Representative cells ($n > 10$) are shown. H shows enlarged lamella region highlighting $MLCK_{125}$ association with actin-like cytoskeletal meshwork. Please refer to Videos 3 and 4 (available at http://www.jcb.org/cgi/content/full/jcb.200110161/DC1) for the dynamic MLCK profile. Arrows show initial tail position. Bar, 5 μm.

### During cytokinesis $MLCK_{125}$ is activated at both the cleavage furrow and the poles

Myosin is dramatically reorganized during cytokinesis, with phosphorylated RLC enriched in the midzone of mitotic spindle during late anaphase, before the constriction of cleavage furrow (Matsumura et al., 1998). $MLCK_{210}$ has been localized to the cleavage furrow and the cortical regions of dividing cells, whereas $MLCK_{125}$ remained diffuse (Poperechnaya et al., 2000). Fig. 6 A shows MLCK-FIP during cytokinesis in transiently transfected NRK cells. MLCK intensity and FRET profile were measured along a dividing cell during cytokinesis (dotted red line) and is shown in Fig. 6 B. Significant MLCK enrichment occurred at late metaphase (indicated by equatorial alignment of chromosomes, phase image not shown) at the equator of the spindle, and showed moderate levels of calmodulin binding. Immediately before constriction of the cleavage furrow at late anaphase (red arrowhead, time: 7:30), $MLCK_{125}$ appeared maximally activated. The surge of activity at the cleavage furrow was immediately followed by recruitment of active $MLCK_{125}$ to the polar regions of the daughter cells. $MLCK_{125}$ intensity at the spindle midzone dropped following the onset of cleavage furrow contraction (Fig. 6 B, left), but was maximally activated until cleavage was complete (Fig. 6 B, right). MLCK at the poles showed high level of calmodulin binding especially within the lamella and ruffles.

## Discussion

To extend our understanding of myosin regulation during cell motility, we produced a biosensor able to both localize MLCK and provide information regarding its activation state in living cells. Since MLCK is regulated by $[Ca^{2+}]_4$/calmodulin binding, we adopted a strategy to detect colocaliza-

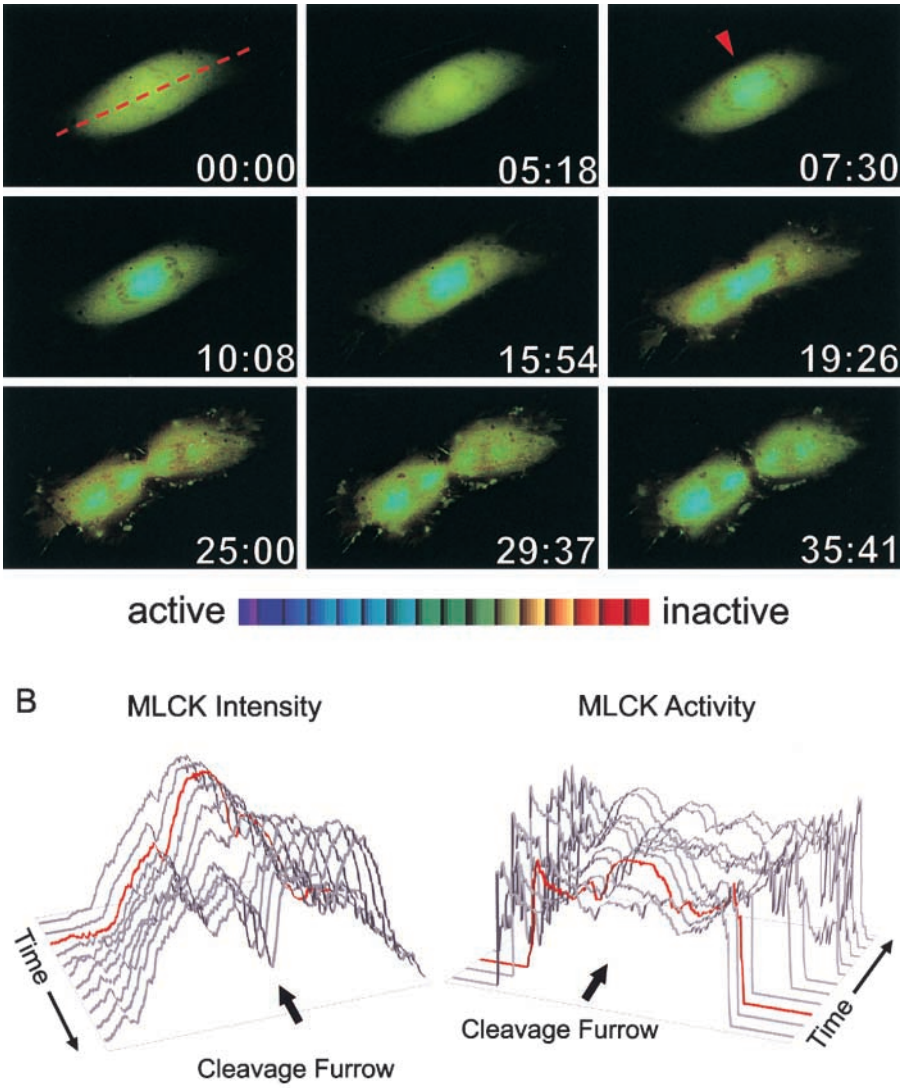


Figure 6. **$MLCK_{125}$ shows bimodal distribution during cell division.** (A) MLCK localization and its state of activation during cell division in a typical NRK cell ($n = 8$). Arrowhead indicates the maximal activation of $MLCK_{125}$ before cleavage furrow contraction. (B) The pixel values along the dashed red line in A were plotted as function of time. $F_{GFP}$ images were used to determine the MLCK-FIP intensity. $F_{FRET}/F_{GFP}$ values indicated MLCK activity. The relative level of MLCK intensity and activity were displayed in arbitrary units on the z-axis height. Red data lines on graphs indicate the onset of cleavage furrow contraction. Note the different directions on the time axis. MLCK localization to the cleavage furrow decreases as cytokinesis continues while MLCK activity increases. Changes in MLCK intensity may reflect changes in thickness of the cell and/or in MLCK concentration. Please refer to Video 5, available at http://www.jcb.org/cgi/content/full/jcb.200110161/DC1.

tion of $MLCK_{125}$ and its activator, $[Ca^{2+}]_4$/calmodulin, by fusing the FIP to the COOH terminus of $MLCK_{125}$. Binding of $[Ca^{2+}]_4$/calmodulin to the regulatory site in MLCK-FIP activates the kinase (Fig. 1 B) while binding to the FIP domain disrupts FRET between the GFP-based donor and acceptor (Fig. 2). We showed that the biosensor retained the regulation and enzymatic properties of that of wild-type MLCK, and detected $[Ca^{2+}]_4$/calmodulin changes in vivo. These results suggest that MLCK-FIP provides an indication of MLCK activation state in living cells.

Several factors affect the accuracy with which MLCK-FIP reports MLCK activation state. The first is the requirement for the two $[Ca^{2+}]_4$/calmodulin binding domains in MLCK-FIP to have similar calmodulin binding properties. Romoser et al. (1997) have shown $[Ca^{2+}]_4$/calmodulin binding to MLCK and FIP to be comparable. A second factor is that MLCK-FIP must accurately reflect the MLCK localization. The most distinctive pattern of MLCK localization is its association with stress fibers (de Lanerolle et al., 1981; Guerriero et al., 1981; Matsumura et al., 1998; Lin et al., 1999; Poperechnaya et al., 2000). As shown in Fig. 3 B, MLCK-FIP shows stress fiber localization. Thus, at least for the most identifiable sites, MLCK-FIP displays the same localization as wild-type MLCK. Third, to accurately reflect activity, MLCK-FIP must also localize to cellular regions with high levels of RLC phosphorylation. Fig. 3 A shows that regions where myosin RLC is most heavily phosphorylated also exhibit high levels of MLCK-FIP activation. There are also regions, particularly the leading edge, where MLCK activity is high but where there is relatively little myosin. The possible reasons for this are discussed below, but there is generally good agreement between higher levels of RLC phosphorylation and MLCK-FIP activation.

Since activation state is inferred from calmodulin binding, could there be situations where calmodulin binding might not accurately reflect MLCK activation? MLCK is phosphorylated by several kinases, including PAK, CaM kinase II, and PKA. CaM kinase II or PKA phosphorylation of Ser-992, which is located in the $[Ca^{2+}]_4$/calmodulin binding domain, decreases $MLCK_{125}$-calmodulin binding efficiency (Payne et al., 1986; Ikebe and Reardon, 1990; Tansey et al., 1992). In addition, bound calmodulin blocks phosphorylation of this site. MLCK is also phosphorylated by PAK at residues Ser-439 and Ser-991 (Goeckeler et al., 2000). Ser-439 phosphorylation has been postulated to affect protein–protein interactions, but there is no direct experimental test

of this idea. Like Ser-992, calmodulin binding blocks PAK-mediated phosphorylation of Ser-991 (Goeckeler et al., 2000). Although it is debatable if PAK phosphorylation reduces calmodulin binding (Sanders et al., 1999), it is easy to imagine that phosphorylation of these sites blocks calmodulin binding and prevents MLCK activation. Ser-991 and Ser-992 are present in both the calmodulin-binding domains of MLCK-FIP. Thus, if PAK, PKA, or CaM kinase II were to phosphorylate these sites in both calmodulin-binding domains, affecting calmodulin binding, the MLCK-FIP would accurately reflect the activation state of MLCK. On the other hand, if phosphorylation were to regulate MLCK independently of calmodulin binding, which has not been demonstrated, MLCK-FIP might not accurately display the MLCK activity. Another case where MLCK-FIP might not accurately reflect MLCK activity is regulation through the nucleotide-binding domain of the MLCK catalytic core, a drug target for inhibitors such as KT-5926. Despite these caveats, our results suggest MLCK-FIP reflects MLCK activity and provides the best tool available to study the dynamic regulation of MLCK in vivo.

### Transient enrichment of calmodulin-bound $MLCK_{125}$ induces contraction

Although MLCK has been directly implicated in mediating cellular contraction in permeabilized endothelial cells (Wysolmerski and Lagunoff, 1991) and isolated stress fibers (Katoh et al., 2001), the dynamic aspects of how MLCK regulates myosin function are poorly understood. This is complicated by the existence of two isoforms of MLCK. The vertebrate MLCK gene produces two kinases (Birukov et al., 1998): (a) a 108–125-kD MLCK ($MLCK_{125}$) found in both smooth muscle and nonmuscle cells; and (b) a 210-kD MLCK ($MLCK_{210}$), expressed in nonmuscle cells, consisting of $MLCK_{125}$ with a 900–amino acid $NH_2$-terminal extension (Poperechnaya et al., 2000). The MLCK-FIP described in this report is based on $MLCK_{125}$, although $MLCK_{210}$-FIP is in development. Since antibodies against $MLCK_{125}$ also recognize $MLCK_{210}$, immunolocalization cannot distinguish between these isoforms. GFP-$MLCK_{210}$ associates with stress fibers with high affinity (Poperechnaya et al., 2000), suggesting it can be activated in situ. GFP-tagged $MLCK_{125}$ localizes differently in different cell types. Poperechnaya et al. (2000) showed $MLCK_{125}$ to be largely diffuse in the cytoplasm, while Lin et al. (1997, 1999) observed filament-bound $MLCK_{125}$. The short MLCK isoform also contains a high affinity actin-binding motif (Smith et al., 1999). Consistent with Lin et al. (1997, 1999), we observed MLCK-FIP in association with stress fibers. We also observed recruitment of additional MLCK-FIP to stress fibers as they contract (Fig. 4). This suggests that stress fiber association of $MLCK_{125}$ may be regulated and transient, providing a basis to reconcile the previous contradictory observations.

Rho kinase has been proposed to induce a slow and sustained contractility to maintain tension along stress fibers, whereas MLCK mediates a rapid but transient contraction (Katoh et al., 2001). The rapid enrichment of $MLCK_{125}$ activity on stress fibers is consistent with in vitro kinetic studies. The $K_m$ of MLCK for RLC is higher than Rho kinase, suggesting that it may work optimally at high local RLC concentration. The high $V_{max}$ of MLCK is ideal to mediate rapid myosin activation. Our studies with MLCK-FIP suggest that localized contraction is mediated by a combination of transient association of MLCK with stress fibers and localized MLCK activation.

### MLCK and directed cell movement

Previous in vitro biochemical studies show that RLC phosphorylation mediates myosin assembly into bipolar filaments (Ikebe et al., 1988; Trybus and Lowey, 1988; Katoh and Morita, 1996). In the leading lamella, apparently diffuse myosin becomes organized into clusters of bipolar filaments (DeBiasio et al., 1988; Verkhovsky and Borisy, 1993; Verkhovsky et al., 1995). Localization of highly activated MLCK-FIP in this region suggests that $MLCK_{125}$ could regulate myosin organization. Consistent with this, reducing MLCK expression limits lamellipodial extension in smooth muscle cells after platelet-derived growth factor treatment (Kishi et al., 2000). Since the protrusion of lamellipodia is driven mainly by actin polymerization (reviewed in Higgs and Pollard, 2001), the mechanism by which myosin contributes to motility in the lamella of a migrating cells is unclear. Fig. 7 presents a model suggested by the observation of activated MLCK in the lamella. Myosin II filaments aggregate in the lamella to form ribbon-like structures that may exert tension required to bundle loosely aligned actin filaments (Verkhovsky et al., 1995). We suggest that MLCK-mediated myosin activation may lead to contraction in the region where myosin spots coalesce to form a meshwork of stress fibers (Fig. 7). Myosin-mediated contraction of the cytoskeleton in this region would exert force between the lamella and cell center as proposed previously (Lauffen-

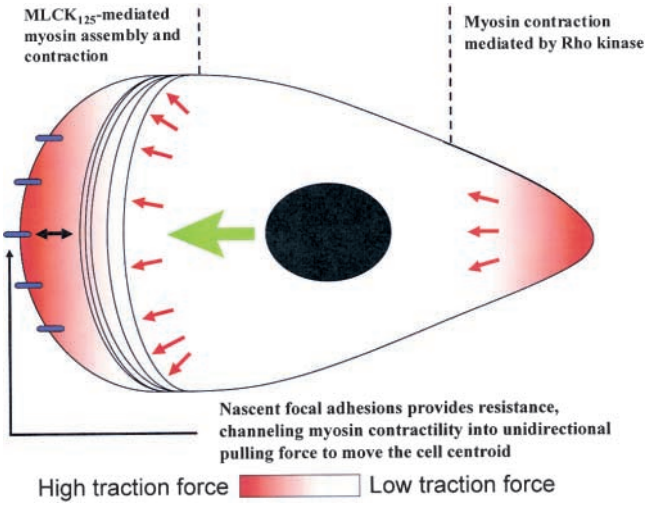


Figure 7. **A model for myosin contraction as a pulling force in motility.** A schematic illustration of how myosin contraction at the front of the nucleus may work synergistically with actin polymerization to facilitate movement. Myosin contraction at the convergence zone generates a bidirectional pulling force, acting on both the leading edge and the cell centroid. The pulling force at the leading front is rendered nonproductive by the nascent focal adhesions, turning myosin contraction into a productive monodirectional force that pulls the centroid forward. Rho kinase–activated myosin may mediate tail retraction.

burger and Horwitz, 1996; Mitchison and Cramer, 1996). Nascent focal complexes at the leading edge withstand large traction forces (Beningo et al., 2001), thus anchoring the lamella. This resistance would convert the myosin-based contraction into a productive force to pull the nucleus toward the leading edge. Thus, myosin contractility in the lamella may work in synergy with actin polymerization to produce directed cell movement.

Myosin activity has been postulated to play a critical role in producing force for tail retraction (Janson and Taylor, 1993; Worthylake et al., 2001). The presence of highly phosphorylated RLC supports this hypothesis (Matsumura et al., 1998). Surprisingly, MLCK activation was seldom observed in the tail region of motile cells. This result raises the interesting possibility that another RLC-targeting kinase may be the primary regulator of myosin activity in the tail. Consistent with this, it has recently been shown that Rho kinase is required and sufficient to mediate monocyte tail retraction during transendothelial migration (Worthylake et al., 2001). These observations highlight the value of MLCK-FIP, and exemplify how motile cells may compartmentalize overlapping signaling events.

### MLCK is activated in cleavage furrow and cortex during cytokinesis

MLCK-FIP has also provided insight into the regulation of cytokinesis. MLCK-FIP was localized to the spindle midzone during late metaphase before its activation. Calcium and calmodulin dynamics complement the MLCK dynamics we observe during cytokinesis. Elevation of free $Ca^{2+}$ begins in anaphase, and persists through daughter cell separation (Tombes and Borisy, 1989). During mitosis, calmodulin is concentrated at the spindle poles and in the cortex (Li et al., 1999). Cortical calmodulin is redistributed to the equator before cleavage furrow formation. Using a sensor (Torok and Trentham, 1994) that detects calmodulin binding to $Ca^{2+}$ and its target, only equatorial calmodulin interacts with downstream effector(s) (Li et al., 1999). Enrichment of $MLCK_{125}$ at the equator before its activation suggests that MLCK localization is not dependent on $[Ca^{2+}]_4$/calmodulin. Interaction between MLCK and $[Ca^{2+}]_4$/calmodulin, indicated by loss of FRET, does not correlate with MLCK-FIP intensity during cytokinesis. These data argue against the possibility that MLCK-FIP is mislocalized to regions of high $[Ca^{2+}]_4$/calmodulin. The differential distribution of $Ca^{2+}$ and calmodulin in cultured mammalian cells led to the suggestion that calmodulin might be involved in positioning of the cleavage furrow (Li et al., 1999). However, the dynamics of MLCK-FIP suggests that the contractile machinery may already be in place, and calmodulin activates contraction locally.

MLCK-FIP accumulated at the midzone until contraction was initiated. During this time, the MLCK became increasingly associated with calmodulin and thus activated (Fig. 6 A, red arrowhead). Once contraction began, the amount of MLCK-FIP in the cleavage furrow began to decrease, although what remained was highly activated (Fig. 6 B). As contraction proceeded, MLCK both accumulated and was activated at the poles. In contrast, $[Ca^{2+}]_4$/calmodulin from the cortical pool is redistributed to the equator (Li et al., 1999). The lack of $[Ca^{2+}]_4$/calmodulin at the poles of the daughter cells suggests that $MLCK_{125}$ may remain active as the kinase translocates from the equator to the poles. Following cleavage furrow contraction, myosin, monitored by GFP-RLC, follows a similar translocation from the furrow to the poles (unpublished data). It is first concentrated at the equator during late metaphase, and then accumulates at the poles after constriction of cleavage furrow has occurred. It is unclear what molecular mechanism is responsible for this redistribution. Perhaps MLCK is transported by the same mechanism as myosin, or even by association with the redistributing myosin.

The localization of active MLCK to the new leading edges of the daughter cells after cytokinesis is consistent with our model that myosin is required for the pulling force between the nucleus and lamellipodia. MLCK recruitment to the poles where extensive cell spreading occurs may activate myosin to facilitate the separation of the two daughter cells in the same way we suggest myosin contractility might pull the nucleus forward during migration.

### Conclusion

Our data have documented the recruitment of MLCK to various cytoskeletal structures during contraction, motility, and cytokinesis. The ability to simultaneously infer MLCK activity from calmodulin binding and monitor its localization highlights the lack of a direct correlation between localization and enzymatic activity, providing an important reminder that the localization of a protein cannot be automatically translated into its activity. The biosensor can easily be adapted to study other $[Ca^{2+}]_4$/calmodulin-dependent proteins in vivo, such as calmodulin-dependent protein kinase II. Understanding the spatio-temporal dynamics of other kinases could advance our understanding of the signal transduction pathways important for directed cell migration.

## Materials and methods

### Generating the MLCK-FIP and wild-type MLCK constructs

Both the BFP and GFP cDNAs were PCR-amplified from the appropriate vectors of the "Living Colors" GFP vector series purchased from CLONTECH Laboratories, Inc. Overlapping primers were designed to join the two fluorophores via a linker GTSS**RRKWNKTGHAVRAIGRLSS**TGA. Bold letters denote the $[Ca^{2+}]_4$/calmodulin binding domain derived from MLCK, whereas the rest of the amino acids are linker sequence. Underlined letters represent $MLCK_{125}$ Ser-991 and Ser-992 equivalents. The FIP cDNA was first subcloned into pcDNA3 vector, to generate the pcDNA3/FIP construct. To fuse the $MLCK_{125}$ cDNA in frame into pcDNA3/FIP, murine $MLCK_{125}$ cDNA (EMBL/GenBank/DDBJ accession no. P29294) was PCR amplified with the downstream primer designed to mutate the stop codon to code for alanine. The $MLCK_{125}$ cDNA was then subcloned into BamHI sites of pcDNA3/FIP, and was sequenced in its entirety to rule out any PCR-related mutation. The final pcDNA3/$MLCK_{125}$-FIP construct contains the murine $MLCK_{125}$ linked to the FIP via a short linker containing the arbitrary amino acid sequence encoded by vector sequence. This construct encodes the 185-kD MLCK-FIP recombinant protein.

To generate the pcDNA3 vector expressing the wild-type $MLCK_{125}$, the murine $MLCK_{125}$ was PCR-amplified to engineer the KpnI and BamHI sites for subcloning into pcDNA3 vector. The positive clones were sequenced to ensure the absence of PCR-related mutation. The construct expresses the 125-kD wild-type $MLCK_{125}$.

### Cell culture and transfection

PTK-2 kangaroo rat epithelial cells (a gift from Dr. Robert Goldman, Northwestern University, Evanston, IL) were cultured in MEM (GIBCO-BRL) supplemented with 10% FCS, and 0.1 mM nonessential amino acids. The nor-

mal rat kidney (NRK) epithelial cell line was a gift from Dr. Yu-Li Wang (University of Massachusetts Medical School, Worcester, MA). NRK cells were cultured in F12 Kaighn's modified medium (Sigma-Aldrich), supplemented with 10% FCS. COS-7 cells were kindly provided by Dr. Kathleen Green (Northwestern University, Evanston, IL) and were maintained in DME supplemented with 10% FCS. All cell lines were maintained in an atmosphere of 5% $CO_2$ at 37°C.

Transfection was performed by electroporation. Cells were trypsinized and pelleted by centrifugation. The cell pellets were resuspended in 1 ml appropriate medium. 200 μl of the resuspended cells were mixed with 7–10 μg DNA containing 13 μg sheared salmon sperm DNA and electroporated in 4-mm cuvettes using Bio-Rad Laboratories Gene Pulser set at 200 ohms, 960 μFD, 250 V. Using this method, we achieved high transfection efficiencies (70–90%) for most cell types at a wide range of cell density except NRK cells, in which ~10–15% could be transfected. Peak protein expression levels observed 18–48 h posttransfection for all cell lines.

### Reagents, proteins, and antibodies

Polyclonal rabbit anti-MLCK antibody and purified $MLCK_{125}$ were provided by Dr. Robert Wysolmerski (St. Louis University, St. Louis, MO). Ionomycin and calmodulin were purchased from Calbiochem. Protein-A sepharose was purchased from Amersham Pharmacia Biotech. pp2b rabbit polyclonal antibody specific for Ser-19–phosphorylated RLC was obtained from Dr. Fumio Matsumura. Monoclonal antimyosin heavy chain antibody was purchased from Covance. Texas red–conjugated goat anti–mouse IgM and Cy5-conjugated donkey anti–rabbit IgG were purchased from Jackson ImmunoResearch Laboratories.

### Protein expression and purification

Myosin II RLC cDNA was cloned into pET14b vector (Novagen) for the expression of His-tagged RLC, and protein expression was induced in BL21 by 0.4 mM IPTG for 3 h. Bacterial pellet was lysed in lysis buffer A (5 mM imidazole, 0.5 NaCl, 20 mM Tris-HCl, pH 7.9) containing 6 M urea and protease inhibitors. Following sonication, cell lysate was precleared by 20,000 *g* centrifugation, and loaded onto His-Bind column (Novagen) preequilibrated with the same buffer. After washing the column with washing buffer A (60 mM imidazole, 0.5 M NaCl, 20 mM Tris-HCl, pH 7.9), protein was eluted using elution buffer A (500 mM imidazole, 250 mM NaCl, 10 mM Tris-HCl, pH 7.9). The eluted protein was dialyzed against dialysis buffer A (20 mM MOPS, pH 7.2, 250 mM NaCl, 1 mM $CaCl_2$, 1 mM $MgCl_2$) with stepwise decrease of imidazole concentration from 500 to 250 mM. Lower imidazole concentration resulted in massive protein precipitation. Cleaving the His tag did not eradicate the precipitation problem.

MLCK-FIP and wild-type MLCK were overexpressed in COS-7 cells for purification. Cell lysates were collected from 16 confluent 10-cm cell culture dishes. Cells were lysed in 35 ml of lysis buffer B (10 mM MOPS, pH 6.8, 5 mM $MgCl_2$, 1.25 mM EGTA, 1 mM EDTA, 10% glycerol, 1% NP-40) containing protease inhibitors. Lysates were sonicated briefly in sonicator waterbath and precleared with 50,000 *g* centrifugation, and purified using Mono-Q ion exchange chromatography preequilibrated with lysis buffer B without NP-40 and glycerol. The column was washed with 2 vol of equilibration buffer and the proteins eluted against a gradient of 0–600 mM NaCl in elution buffer B (10 mM MOPS, pH 6.8, 5 mM $MgCl_2$, 1.25 mM EGTA, 1 mM EDTA). Analysis of the elution profile showed that MLCK-FIP and wild-type MLCK were reproducibly eluted three fractions apart from one another, thus allowing us to separate MLCK-FIP from endogenous wild-type MLCK.

### In vitro FRET analysis

In vitro spectrofluorimetric analysis of MLCK-FIP was performed using an AMINCO Bowman Series 2 Luminescence Spectrometer. An excitation wavelength of 380 nm was used throughout the experiment. Purified MLCK-FIP was assayed in 1 ml reaction mixture containing 20 mM MOPS buffer, pH 7.2, 10 mM NaCl, 1 mM EDTA, 1 mM EGTA, and 1 μM calmodulin. Standard $CaCl_2$ solution was added to the cuvette to titrate the effects of increasing $[Ca^{2+}]_4$/calmodulin. The free $Ca^{2+}$ available for binding to calmodulin is calculated by MaxChelator program, taking into account all divalent cations and their chelators in the buffer. An emission scan from 430 nm to 540 nM was performed with each addition of $CaCl_2$.

### RLC phosphorylation

To compare the rate of RLC phosphorylation catalyzed by MLCK-FIP with that by wild-type MLCK, the recombinant kinases were transiently overexpressed in COS-7 cells and immunoprecipitated using rabbit polyclonal anti-MLCK antibody. The amount of immunoprecipitated MLCK was estimated by comparing the densitometric units of the MLCK bands on immunoblot to that of a standard curve set up by varying amount of recombinant $MLCK_{125}$. Immunoprecipitate containing 1 μg kinase was used in the in vitro kinase assay. The fact that our recombinant RLC precipitates at low salt and high protein concentration precludes the accurate determination of Vmax and Km by conventional method. Instead we compared the rate of phosphorylation by MLCK-FIP and wild-type MLCK at three substrate concentrations. Kinase assay was performed in 25 mM Tris-HCl, pH 7.5, 5 mM $MgCl_2$, 1 mM DTT, 0.5 mM $CaCl_2$, 100 mM KCl, and 1 μM calmodulin. Specific activity of $^{32}$P-γ-ATP was 4,000 cpm/pmole. 5 μl of the reaction was removed at the indicated time points and spotted onto Whatman P81 ion exchange paper, and the reaction stopped by ice-cold 10% trichloroacetic acid containing 2% sodium pyrophosphate. The papers were washed four times in ice-cold acetone, heated to 80°C for 15 min, and washed once with acetone to remove heat-labile phosphate. The samples were then counted in scintillation counter.

### Live cell imaging

Live cell imaging was performed on ZEISS Axiovert S100-TV inverted fluorescent microscope. Rapid switching of fluorescent wavelength was accomplished by emission and excitation filter wheels controlled by Sutter Instruments Lambda 10 controller, and the shutters were controlled by Uniblitz VMM-D1 shutter drivers. Digital fluorescent images were captured by Micromax cooled CCD camera (Princeton Instruments) with a 512 × 512 camera chip. Filter wheels are equipped with bandpass filters for BFP and GFP with a stationary dual beamsplitter for BFP and GFP located in the filter block. Filters were purchased from Chroma. Live cells were imaged in a Bioptechs FCS2 closed chamber system maintained at 37°C, with a chamber thickness of 0.75 mm. To reduce the background fluorescence and to image cell in the absence of $CO_2$, the cell medium was mixed with equal volume of Leibovitz L-15 medium without Phenol Red (GIBCO-BRL) supplemented with 10% FCS. Fresh medium was perfused at 0.1 ml/min into the chamber during imaging.

Cell images were taken using MetaMorph 4.5 (Universal Imaging Corp.) software. The images were taken with 200–300 ms exposure with ~50 ms interval between the numerator $F_{FRET}$ and the denominator $F_{GFP}$ images. Ratio images were constructed by displaying the ratio in 16 different color hues with the lowest ratio (MLCK active) displayed at the blue end of the ratio spectrum. Using the intensity of the denominator (which served as the internal control irrespective of FRET), the ratio colors were displayed in sixteen different intensity levels by the Intensity Modulatory Display mode (Fig. 2 B). Therefore, depending on the enrichment and the activation state of MLCK-FIP at any given subcellular region, the color of the ratio denotes the relative extent at which MLCK-FIP associates with $[Ca^{2+}]_4$/calmodulin, while the intensity of that ratio color represents the amount of MLCK-FIP being localized by the cell. To highlight the dynamic recruitment of $MLCK_{125}$ to cytoskeletal structures, FRET ratio was plotted against the intensity profile, whereby the pixel intensity was represented by line height, and the FRET ratio depicted by the line color. We have avoided cells with saturated pixels to minimize error on ratio calculation.

To correlate the relative activity of MLCK-FIP with the extent of RLC phosphorylation in vivo, PTK-2 cells transiently expressing MLCK-FIP were plated on gridded coverslips. The ratio images of MLCK-FIP were obtained as described, and the cells were immediately fixed. The coverslips were blocked with PBS containing 0.1% BSA and 1:20 dilution of normal goat serum. Double immunofluorescence was performed with antimyosin mAb and pp2b polyclonal antiphosphorylated RLC antibody. Primary antibody incubation performed at 37°C for 1 h. After washing in PBS, the secondary antibody was performed at 37°C for 30 min with Texas red–conjugated goat anti–mouse IgM, and Cy5-conjugated donkey anti–rabbit IgG. Immunolocalization images were taken with ZEISS LSM 510 confocal microscope and ratio of the images performed on MetaMorph 4.5.

### Online supplemental materials

There are videos relating to Figs. 4–6 available online. Video 1 corresponds to Fig. 4, A–D; Video 2 corresponds to Fig. 4, E–H; Video 3 corresponds to Fig. 5, A–D; Video 4 corresponds to Fig. 5, E–H; and Video 5 corresponds to Fig. 6.

We thank Dr. Steve Adam for his help in MLCK purification and Satya Khuon for her assistance in confocal microscopy. We are grateful for the numerous reagents supplied by Dr. Robert Wysolmerski.

This work was supported by National Institutes of Health Grant GM39264 (to R.L. Chisholm) and Department of Defense Breast Cancer Fellowship DAMD17-00-1-0385 (to T.-L. Chew).

Submitted: 31 October 2001
Revised: 21 December 2001
Accepted: 2 January 2002

## References

Amano, M., M. Ito, K. Kimura, Y. Fukata, K. Chihara, T. Nakano, Y. Matsuura, and K. Kaibuchi. 1996. Phosphorylation and activation of myosin by Rho-associated kinase (Rho-kinase). *J. Biol. Chem.* 271:20246–20249.

Beningo, K.A., M. Dembo, I. Kaverina, J.V. Small, and Y.L. Wang. 2001. Nascent focal adhesions are responsible for the generation of strong propulsive forces in migrating fibroblasts. *J. Cell Biol.* 153:881–888.

Birukov, K.G., J.P. Schavocky, V.P. Shirinsky, M.V. Chibalina, L.J. Van Eldik, and D.M. Watterson. 1998. Organization of the genetic locus for chicken myosin light chain kinase is complex: multiple proteins are encoded and exhibit differential expression and localization. *J. Cell. Biochem.* 70:402–413.

Chew, T.L., R. Masaracchia, and R. Wysolmerski. 1998. Phosphorylation of non-muscle myosin II regulatory light chain by p21- activated kinase (γ-PAK). *J. Muscle Res. Cell Motil.* 19:839–854.

Chrzanowska-Wodnicka, M., and K. Burridge. 1996. Rho-stimulated contractility drives the formation of stress fibers and focal adhesions. *J. Cell Biol.* 133: 1403–1415.

de Lanerolle, P., R.S. Adelstein, J.R. Feramisco, and K. Burridge. 1981. Characterization of antibodies to smooth muscle myosin kinase and their use in localizing myosin kinase in nonmuscle cells. *Proc. Natl. Acad. Sci. USA.* 78: 4738–4742.

DeBiasio, R.L., L.L. Wang, G.W. Fisher, and D.L. Taylor. 1988. The dynamic distribution of fluorescent analogues of actin and myosin in protrusions at the leading edge of migrating Swiss 3T3 fibroblasts. *J. Cell Biol.* 107:2631–2645.

Goeckeler, Z.M., R.A. Masaracchia, Q. Zeng, T.L. Chew, P. Gallagher, and R.B. Wysolmerski. 2000. Phosphorylation of myosin light chain kinase by p21-activated kinase PAK2. *J. Biol. Chem.* 275:18366–18374.

Goeckeler, Z.M., and R.B. Wysolmerski. 1995. Myosin light chain kinase-regulated endothelial cell contraction: the relationship between isometric tension, actin polymerization, and myosin phosphorylation. *J. Cell Biol.* 130: 613–627.

Guerriero, V., Jr., D.R. Rowley, and A.R. Means. 1981. Production and characterization of an antibody to myosin light chain kinase and intracellular localization of the enzyme. *Cell.* 27:449–458.

Higgs, H.N., and T.D. Pollard. 2001. Regulation of actin filament network formation through Arp2/3 complex: activation by a diverse array of proteins. *Annu. Rev. Biochem.* 70:649–676.

Ikebe, M., and D.J. Hartshorne. 1985. Phosphorylation of smooth muscle myosin at two distinct sites by myosin light chain kinase. *J. Biol. Chem.* 260:10027–10031.

Ikebe, M., D.J. Hartshorne, and M. Elzinga. 1986. Identification, phosphorylation, and dephosphorylation of a second site for myosin light chain kinase on the 20,000-dalton light chain of smooth muscle myosin. *J. Biol. Chem.* 261:36–39.

Ikebe, M., D.J. Hartshorne, and M. Elzinga. 1987. Phosphorylation of the 20,000-dalton light chain of smooth muscle myosin by the calcium-activated, phospholipid-dependent protein kinase. Phosphorylation sites and effects of phosphorylation. *J. Biol. Chem.* 262:9569–9573.

Ikebe, M., J. Koretz, and D.J. Hartshorne. 1988. Effects of phosphorylation of light chain residues threonine 18 and serine 19 on the properties and conformation of smooth muscle myosin. *J. Biol. Chem.* 263:6432–6437.

Ikebe, M., and S. Reardon. 1990. Phosphorylation of smooth myosin light chain kinase by smooth muscle Ca2+/calmodulin-dependent multifunctional protein kinase. *J. Biol. Chem.* 265:8975–8978.

Janson, L.W., and D.L. Taylor. 1993. In vitro models of tail contraction and cytoplasmic streaming in amoeboid cells. *J. Cell Biol.* 123:345–356.

Katoh, K., Y. Kano, M. Amano, H. Onishi, K. Kaibuchi, and K. Fujiwara. 2001. Rho-kinase–mediated contraction of isolated stress fibers. *J. Cell Biol.* 153:569–584.

Katoh, T., and F. Morita. 1996. Roles of light chains in the activity and conformation of smooth muscle myosin. *J. Biol. Chem.* 271:9992–9996.

Kishi, H., T. Mikawa, M. Seto, Y. Sasaki, T. Kanayasu-Toyoda, T. Yamaguchi, M. Imamura, M. Ito, H. Karaki, J. Bao, et al. 2000. Stable transfectants of smooth muscle cell line lacking the expression of myosin light chain kinase and their characterization with respect to the actomyosin system. *J. Biol. Chem.* 275:1414–1420.

Lauffenburger, D.A., and A.F. Horwitz. 1996. Cell migration: a physically integrated molecular process. *Cell.* 84:359–369.

Li, C.J., R. Heim, P. Lu, Y. Pu, R.Y. Tsien, and D.C. Chang. 1999. Dynamic redistribution of calmodulin in HeLa cells during cell division as revealed by a GFP-calmodulin fusion protein technique. *J. Cell Sci.* 112:1567–1577.

Lin, P., K. Luby-Phelps, and J.T. Stull. 1997. Binding of myosin light chain kinase to cellular actin-myosin filaments. *J. Biol. Chem.* 272:7412–7420.

Lin, P., K. Luby-Phelps, and J.T. Stull. 1999. Properties of filament-bound myosin light chain kinase. *J. Biol. Chem.* 274:5987–5994.

Matsumura, F., S. Ono, Y. Yamakita, G. Totsukawa, and S. Yamashiro. 1998. Specific localization of serine 19 phosphorylated myosin II during cell locomotion and mitosis of cultured cells. *J. Cell Biol.* 140:119–129.

Mishima, M., and I. Mabuchi. 1996. Cell cycle-dependent phosphorylation of smooth muscle myosin light chain in sea urchin egg extracts. *J. Biochem. (Tokyo).* 119:906–913.

Mitchison, T.J., and L.P. Cramer. 1996. Actin-based cell motility and cell locomotion. *Cell.* 84:371–379.

Payne, M.E., M. Elzinga, and R.S. Adelstein. 1986. Smooth muscle myosin light chain kinase. Amino acid sequence at the site phosphorylated by adenosine cyclic 3′,5′-phosphate-dependent protein kinase whether or not calmodulin is bound. *J. Biol. Chem.* 261:16346–16350.

Poperechnaya, A., O. Varlamova, P. Lin, J.T. Stull, and A.R. Bresnick. 2000. Localization and activity of myosin light chain kinase isoforms during the cell cycle. *J. Cell Biol.* 151:697-708.

Romoser, V.A., P.M. Hinkle, and A. Persechini. 1997. Detection in living cells of Ca2+-dependent changes in the fluorescence emission of an indicator composed of two green fluorescent protein variants linked by a calmodulin-binding sequence. A new class of fluorescent indicators. *J. Biol. Chem.* 272: 13270–13274.

Sanders, L.C., F. Matsumura, G.M. Bokoch, and P. de Lanerolle. 1999. Inhibition of myosin light chain kinase by p21-activated kinase. *Science.* 283:2083–2085.

Satterwhite, L.L., M.J. Lohka, K.L. Wilson, T.Y. Scherson, L.J. Cisek, J.L. Corden, and T.D. Pollard. 1992. Phosphorylation of myosin-II regulatory light chain by cyclin-p34cdc2: a mechanism for the timing of cytokinesis. *J. Cell Biol.* 118:595–605.

Sellers, J.R., M.D. Pato, and R.S. Adelstein. 1981. Reversible phosphorylation of smooth muscle myosin, heavy meromyosin, and platelet myosin. *J. Biol. Chem.* 256:13137–13142.

Smith, L., X. Su, P. Lin, G. Zhi, and J.T. Stull. 1999. Identification of a novel actin binding motif in smooth muscle myosin light chain kinase. *J. Biol Chem.* 274:29433–29438.

Tansey, M.G., R.A. Word, H. Hidaka, H.A. Singer, C.M. Schworer, K.E. Kamm, and J.T. Stull. 1992. Phosphorylation of myosin light chain kinase by the multifunctional calmodulin-dependent protein kinase II in smooth muscle cells. *J. Biol. Chem.* 267:12511–12516.

Tombes, R.M., and G.G. Borisy. 1989. Intracellular free calcium and mitosis in mammalian cells: anaphase onset is calcium modulated, but is not triggered by a brief transient. *J. Cell Biol.* 109:627–636.

Torok, K., and D.R. Trentham. 1994. Mechanism of 2-chloro-(epsilon-amino-Lys75)-[6-[4-(N,N-diethylamino)phenyl]-1,3,5-triazin-4-yl]calmodulin interactions with smooth muscle myosin light chain kinase and derived peptides. *Biochemistry.* 33:12807–12820.

Trybus, K.M., and S. Lowey. 1988. The regulatory light chain is required for folding of smooth muscle myosin. *J. Biol. Chem.* 263:16485–16492.

Tsien, R.Y., and A.T. Harootunian. 1990. Practical design criteria for a dynamic ratio imaging system. *Cell Calcium.* 11:93–109.

Turbedsky, K., T.D. Pollard, and A.R. Bresnick. 1997. A subset of protein kinase C phosphorylation sites on the myosin II regulatory light chain inhibits phosphorylation by myosin light chain kinase. *Biochemistry.* 36:2063–2067.

Verkhovsky, A.B., and G.G. Borisy. 1993. Non-sarcomeric mode of myosin II organization in the fibroblast lamellum. *J. Cell Biol.* 123:637–652.

Verkhovsky, A.B., T.M. Svitkina, and G.G. Borisy. 1995. Myosin II filament assemblies in the active lamella of fibroblasts: their morphogenesis and role in the formation of actin filament bundles. *J. Cell Biol.* 131:989–1002.

Worthylake, R.A., S. Lemoine, J.M. Watson, and K. Burridge. 2001. RhoA is required for monocyte tail retraction during transendothelial migration. *J. Cell Biol.* 154:147–160.

Wysolmerski, R.B., and D. Lagunoff. 1991. Regulation of permeabilized endothelial cell retraction by myosin phosphorylation. *Am. J. Physiol.* 261:C32–C40.

Zeng, Q., D. Lagunoff, R. Masaracchia, Z. Goeckeler, G. Cote, and R. Wysolmerski. 2000. Endothelial cell retraction is induced by PAK2 monophosphorylation of myosin II. *J. Cell Sci.* 113:471–482.